Reduced Order Observer for Structure from Motion using Concurrent Learning

Ghananeel Rotithor, Daniel Trombetta, Rushikesh Kamalapurkar, Ashwin Dani

***Abstract*—In this paper, a concurrent learning based reduced order observer for a perspective dynamical system (PDS) is developed. The PDS is a widely used model for estimating the depth of a feature point from a sequence of camera images. Leveraging the recent advances in concurrent learning for adaptive control, the depth observer is developed for a PDS model where the inverse depth appears as a time varying parameter in the dynamics. Using the data recorded over a sliding time window in the near past, information about the recent depth values is used in a CL term and an observer is developed. A Lyapunov-based stability analysis is carried out to prove the uniformly ultimately bounded (UUB) stability of the observer. Simulations demonstrate the convergence using MAPE and RMSE metrics in the presence and absence of persistence of excitation (PE).**

I. Introduction

In the computer vision literature, the Structure from Motion (SFM) problem involves using observations from a sequence of camera images to estimate the 3D coordinates of feature points. This form of 3D structure reconstruction can be applied to a variety of automatic control, autonomy, and intelligent control scenarios. There exist both offline [1] and online [2]–[5] solutions to the SfM problem. This paper focuses on online methods, wherein the problem is to estimate the state of a perspective dynamical system (PDS), a class of nonlinear system that uses inverse depth parametrization, frequently used in observer-based methods and simultaneous localization and mapping (SLAM).

While, often times, the Extended Kalman Filter (EKF) serves as the backbone for online SfM solutions [6]–[9], other nonlinear observers, both continuous and discontinuous, have been developed with analytical proofs of stability, contingent on known camera motion. Examples of such observers include a high-gain observer called the identifier-based observer (IBO) for range estimation [10], a semi-globally asymptotically stable reduced-order observer to estimate the range of a stationary object [11], a continuous observer which guarantees asymptotic range estimation [12], an asymptotically converging nonlinear observer based on Lyapunov's indirect method [13], a discontinuous sliding-mode observer which guarantees a uniformly ultimately bounded (UUB) result of estimation error to a small ball around the origin of the system [14], and in DeLuca et. al [15], a nonlinear observer that achieves exponentially fast convergence of estimation error provided a persistency of excitation (PE) condition is satisfied. For this observer, a local exponential stability of estimation error dynamics is obtained which requires the initial condition of the observer to be close to the 'true' depth. It is used in conjunction with visual servoing for simultaneous depth estimation and VS control. An immersion and invariance (I&I)-based approach is used in [16] to design a reduced-order observer that achieves global exponential convergence of the estimation error. Velocity and acceleration measurements are required in this observer as well as image feature point measurements. Additionally, the Extended Output Jacobian (EOJ) observability rank condition must be satisfied, which is more strict than the PE condition.

Progressing from our previous work [17]–[19], in which we have developed a globally exponentially stable observer for feature point depth estimation of static objects using a moving camera, this paper presents a concurrent learning (CL)-based state observer designed for a PDS. CL, which is used in adaptive control for parameter estimation, leverages knowledge of past trajectory data to estimate a constant parameter. In a PDS, the inverse depth appears in the dynamics of pixel coordinates as a time-varying parameter with known dynamics associated with it. In this paper, an observer inspired by recent advances in CL for adaptive control [20]–[22] is designed for a PDS which uses CL terms in the observer design. To the authors' knowledge this is the first attempt to incorporate CL terms in the state observer structure.

CL uses a history stack, consisting of recorded input and output data, to update the parameter estimation problem. This allows for a finite duration of excitation while still guaranteeing convergence, thus, relaxing the PE condition to a finite excitation condition. This new condition requires the minimum singular value of the regressor matrix to be positive [23], therefore, allowing the adherence to the condition to be monitored online. This is not possible for the PE condition. CL-based methods have been shown to be advantageous in a variety of applications in which parameter estimation is critical [24]–[26] such as parameter estimation in model reference adaptive control (MRAC) [22], parameter estimation using dynamic state derivatives [21], and simultaneous state and parameter estimation [27].

The existing observers designed for PDS in the literature require a strict PE condition to guarantee the stability of the observer. The PE condition requirement on the convergence

Ghananeel Rotithor, Daniel Trombetta and Ashwin P. Dani are with the Department of Electrical and Computer Engineering at University of Connecticut, Storrs, CT 06269. Email: {ghananeel.rotithor; daniel.trombetta; ashwin.dani}@uconn.edu. Rushikesh Kamalapurkar is with the Mechanical and Aerospace Engineering Department at the Oklahoma State University, OK.

of the observer is relaxed by adding the concurrent learning terms that keep record of past history of depth values. Although, contrary to standard adaptive control, the depth parameter χ is time-varying, the recent past history of the system contains information about the current χ. The simulation results of the new observer design show convergence when PE is violated for a short time duration.

II. Perspective Camera Motion Model

The movement of a camera capturing a scene results in a change of location of a static object in the image plane. Let $\bar{m}(t) \in \mathbb{R}^3$ and $m(t) \in \mathbb{R}^3$ be the Euclidean and normalized Euclidean coordinates, of a point belonging to a static object captured by a moving camera with known velocities

$$\bar{m}(t) = [X, Y, Z]^T \tag{1}$$

$$m(t) = [\frac{X}{Z}, \frac{Y}{Z}, 1]^T \tag{2}$$

where Z is the depth of a point. To estimate the depth, define an auxiliary vector $y(t) \in \mathbb{R}^3$, given by

$$y(t) = [\frac{X}{Z}, \frac{Y}{Z}, \frac{1}{Z}]^T \tag{3}$$

Let $s \in \mathbb{R}^{2m}$ be a collection of m feature points where each feature point s_i has two components. For a single feature point, by formulating the state as $s_i = [y_1(t), y_2(t)]^\intercal$ and inverse depth is $\chi = y_3(t)$, and taking the time derivative of (3), the dynamics of s as a function of linear and angular velocities of the camera can be expressed as

$$\dot{s} = L_s(s, \chi)u \tag{4}$$

where $L_s \in \mathbb{R}^{2m\times 6}$ is the interaction matrix representing the dynamics associated with the feature point, $\chi \in \mathbb{R}^m$ is a vector containing the inverse depth values associated with each feature point, $u \in \mathbb{R}^6$ is a vector of 3-dimensional linear and angular velocities of the camera, defined as $u = [v_X, v_Y, v_Z, \omega_X, \omega_Y, \omega_Z]^T$, where $v = [v_X, v_Y, v_Z]^T \in \mathbb{R}^3$ is the linear velocity and $\omega = [\omega_X, \omega_Y, \omega_Z]^T \in \mathbb{R}^3$ is the angular velocity of the camera. The dynamics in (4) can split into two parts for convenience

$$\dot{s} = f_m(s, \omega) + \Omega^\intercal(s, v)\chi \tag{5}$$

where $f_m(s, \omega) \in \mathbb{R}^{2m}$ and $\Omega(s, v) \in \mathbb{R}^{m\times 2m}$ are functions of measurable quantities or known quantities. The dynamics associated with the inverse depth χ can be modeled as

$$\dot{\chi} = f_u(s, \chi, u) \tag{6}$$

where $f_m(s, \omega) = [-p_1, -p_2]^T$, $\Omega(s, v) = [-h_1, -h_2]$ and $f_u(s, \chi, u) = y_3^2 v_Z + y_2 y_3 \omega_X - y_1 y_3 \omega_Y$. Where p_1, p_2, h_1, h_2 are defined as

$$\begin{aligned} p_1 &= -y_1 y_2 \omega_X + (1 + y_2^2) - y_2 \omega_Z \\ p_2 &= -(1 + y_2^2)\omega_X + y_1 y_2 \omega_Y + y_1 \omega_Z \\ h_1 &= -y_1 v_Z + v_X \\ h_2 &= -y_2 v_Z + v_Y \end{aligned} \tag{7}$$

For the complete derivation from (2)-(7) refer [28] .

Problem Definition: Given the feature point dynamics in (5), the measurements of feature points in images $s_n = [y_1 + \epsilon_X, y_2 + \epsilon_Y]^T$, where ϵ_X and ϵ_Y are additive Gaussian white noise in X and Y direction, and linear and angular velocity of camera u, the depth of each feature point can be estimated using a sequence of image observations of the same feature point. To this end, a depth observer is designed in Section III using concurrent learning (CL).

III. Concurrent Learning-based Observer Design

The depth estimation schemes in the existing literature require a strong observability condition called Persistence of Excitation (PE). For such observers the estimation error converges to zero only if the PE condition is satisfied. In cases where PE cannot be satisfied the observer may be unstable. The PE condition is satisfied if there exists $T, \rho \in \mathbb{R}^+$ for the following integral condition

$$\int_t^{t+T} \Omega(\tau)\Omega^\intercal(\tau)d\tau \geq \rho I > 0, \forall t > t_0 \tag{8}$$

PE is a strict integral condition and is difficult to continuously monitor during simulations and experiments. Concurrent learning based parameter estimation schemes use the recorded data generated by the system to make updates to the parameter estimation dynamics. Thus, the machinery developed in [23] guarantees convergence.

Define the depth estimate of χ as $\hat{\chi}$ and the depth estimation error as $e = \chi - \hat{\chi}$. Using the dynamics in (5) and (6), the observer for estimating the depth is designed as follows.

$$\begin{aligned} \dot{\hat{\chi}} = f_u(s, \hat{\chi}, u) + \bar{K} \sum_{j=1}^{M} \Omega(s_j, v_j)(\dot{s}_j \\ - f_m(s_j, \omega_j) - \Omega^\intercal(s_j, v_j)\hat{\chi}) \end{aligned} \tag{9}$$

where $\bar{K} \in \mathbb{R}^+$ is a suitable observer gain. The index M in (9) is for the signals at the current time instance. Using the system dynamics in (5)-(6) and the observer in (5), the estimation error dynamics can be written as follows.

$$\begin{aligned} \dot{e} = -\bar{K} \sum_{j=1}^{M} \Omega(s_j, v_j)(\dot{s}_j - f_m(s_j, \omega_j) \\ - \Omega^\intercal(s_j, v_j)\hat{\chi}) + g(s, \chi, \hat{\chi}, u) \end{aligned} \tag{10}$$

where $g(s, \chi, \hat{\chi}, u) = f_u(s, \chi, u) - f_u(s, \hat{\chi}, u)$. The state derivative term $\dot{s}(t)$, i.e., the optical flow, can be substituted as $\dot{s}_j = f_m(s_j, \omega_j) + \Omega^\intercal(s_j, v_j)\chi_j$. The error dynamics in (10) can be rewritten as

$$\dot{e} = -\bar{K}\sum_{j=1}^{M}\Omega(s_j,v_j)\Omega^{\intercal}(s_j,v_j)(\chi_j-\hat{\chi}) + g(s,\chi,\hat{\chi},u) \tag{11}$$

Adding and subtracting $\Omega(s_j,v_j)\Omega^{\intercal}(s_j,v_j)\chi$ in the summation term of (11) and combining χ and $\hat{\chi}$

$$\dot{e} = -\bar{K}\big(\sum_{j=1}^{M}\Omega(s_j,v_j)\Omega^{\intercal}(s_j,v_j)e + \sum_{j=1}^{M}\Omega(s_j,v_j)\Omega^{\intercal}(s_j,v_j)(\chi_j-\chi)\big) + g(s,\chi,\hat{\chi},u) \tag{12}$$

Assumption 1: The change in the depth is relatively small, i.e., $\|(\chi_j-\chi)\| \leq \bar{\chi}$, where χ_j are the true depth values during the period $t-t_1$ to t.

IV. Integrated Reduced Order Observer

In situations where the state is completely known or measurable, a reduced order observer can be used. In the context of PDS, the state can be represented by the pixel coordinates of the feature points and can be directly measured from every frame using established computer vision methods for feature point detection. A reduced order observer structure using equation (9) is presented. The observer structure presented in (9) heavily relies on the state derivative $\dot{s}$ which can be noisy due to the computation of optical flow or numerical differentiation. To eliminate the dependency on $\dot{s}$ the observer equation is integrated over time

$$\hat{\chi} = \int_{\tau=0}^{t}(f_u(s(\tau),\hat{\chi}(\tau),u(\tau)) + \bar{K}\sum_{j=1}^{M}\Omega(s_j(\tau),v_j(\tau))(\dot{s}_j(\tau)-f_m(s_j(\tau),\omega_j(\tau)) - \Omega^{\intercal}(s_j(\tau),v_j(\tau))\hat{\chi}(\tau)))d\tau \tag{13}$$

The final reduced observer, can be written as combination of the following two terms

$$\hat{\chi} = \kappa + \beta \tag{14}$$

where

$$\dot{\kappa} = v_Z\hat{\chi}^2 + (y_2\omega_X - y_1\omega_Y)\hat{\chi} + \bar{K}\sum_{j=1}^{M}(y_{1_j}\dot{v}_{X_j} + y_{2_j}\dot{v}_{Y_j} - (h_{1_j}p_{1_j} + h_{2_j}p_{2_j}) - (h_{1_j}^2 + h_{2_j}^2)\hat{\chi} - \frac{y_{1_j}^2\dot{v}_{Z_j} + y_{2_j}^2\dot{v}_{Z_j}}{2}) \tag{15}$$

and

$$\beta = \bar{K}\sum_{j=1}^{M}v_{Z_j}\frac{(y_{1_j}^2 + y_{2_j}^2)}{2} - y_{1_j}v_{X_j} - y_{2_j}v_{Y_j} \tag{16}$$

Notice that the subscript j accompanying velocities and states indicates the j^{th} point in the history stack out of M total points, where the last point is the current point. It is also evident from the final observer structure that the dependency on the state derivative is eliminated as linear accelerations are used instead.

V. Stability Analysis

The stability analysis is carried out for the initial phase where the data is being collected in the history stack of the concurrent learning term and the phase where the history stack is full. In Theorem 1, based on our prior work in [18], it is shown that the estimation error dynamics in (10) is stable under a PE condition. In Theorem 2, it is shown that the estimation error dynamics in (10) yields uniformly ultimately bounded error. The advantage of adding the CL term is that the error is bounded even if the PE is not satisfied.

Theorem 1. *When the history stack is incomplete, the error system in (10) is uniformly ultimately bounded if Assumption 1 and the PE condition in (8) are satisfied.*

Proof: The error system in (12) can be written

$$\dot{e} = -\bar{K}\Omega(s_M,v_M)\Omega^{\intercal}(s_M,v_M)e + g(s,\chi,\hat{\chi},u) - \bar{K}(\sum_{j=1}^{M-1}\Omega(s_j,v_j)\Omega^{\intercal}(s_j,v_j)e + \sum_{j=1}^{M}\Omega(s_j,v_j)\Omega^{\intercal}(s_j,v_j)(\chi_j-\chi)) \tag{17}$$

In the subsequent development the result of Theorem 2 of [18] is used which proves that the error system in (17) without last two terms is globally exponentially stable.

Consider a domain $\mathcal{D}\subset\mathbb{R}^m$ which is continuously differentiable, radially unbounded candidate Lyapunov function, $V(e):\mathcal{D}\to\mathbb{R}^+$, defined as

$$V = \frac{1}{2}e^{\intercal}e \tag{18}$$

The Lyapunov function can be upper and lower bounded by $c_1\|e\|^2 \leq \|V\| \leq c_2\|e\|^2$, where $c_1\in\mathbb{R}$ and $c_2\in\mathbb{R}$ are positive constants. Taking the time derivative of (18) and substituting the error dynamics in (10) and (17) yields

$$\dot{V} = -\bar{K}e^{\intercal}(\Omega(s_M,v_M)\Omega^{\intercal}(s_M,v_M))e + e^{\intercal}g(s,\chi,\hat{\chi},u) - \bar{K}e^{\intercal}(\sum_{j=1}^{M-1}\Omega(s_j,v_j)\Omega^{\intercal}(s_j,v_j)e + \sum_{j=1}^{M}\Omega(s_j,v_j)\Omega^{\intercal}(s_j,v_j)(\chi_j-\chi)) \tag{19}$$

Manuscript 1865 submitted to 2019 IEEE Conference on Decision and Control (CDC).
Received March 17, 2019.

When the history stack is incomplete, $\sum_{j=1}^{M-1} \Omega(s_j, v_j)\Omega^\intercal(s_j, v_j) \geq 0$. Using Assumption 1, (19) can be written as

$$\begin{aligned}\dot{V} \leq & -\bar{K}e^\intercal\Omega(s_M, v_M)\Omega^\intercal(s_M, v_M)e \\ & + e^\intercal g(s, \chi, \hat{\chi}, u) + \bar{K}\sigma_1^2 M\bar{\chi}||e|| \end{aligned} \tag{20}$$

The above equation can be upper bounded as

$$\dot{V} \leq -k_1||e||^2 + k_3||e||$$

where $k_3 = \bar{K}\sigma_1^2 M\bar{\chi}$. Since $k_3 \geq 0$ and the PE condition is satisfied in (20), using the result of Theorem 2 of [18], $\dot{V} \leq -\bar{k}_1||e||^2 \quad \forall||e|| \geq \frac{k_3}{\theta}$, which yields a uniformly ultimately bound on estimation error $\|e(t)\|$ according to Theorem 4.18 of [29]. Where $\bar{k}_1 = k_1 - \theta$. ■

Theorem 2. *When the history stack is complete and full rank, the error system in (10) is uniformly ultimately bounded if Assumption 1 is satisfied.*

Proof: Consider the same candidate Lyapunov function, $V(e) : \mathcal{D} \to \mathbb{R}^+$, in (18). Taking the time derivative of (18) and substituting the error dynamics in (10) and (12) yields

$$\begin{aligned}\dot{V} = & -\bar{K}e^\intercal(\sum_{j=1}^{M}\Omega(s_j, v_j)\Omega^\intercal(s_j, v_j)e \\ & + \sum_{j=1}^{M}\Omega(s_j, v_j)\Omega^\intercal(s_j, v_j)(\chi_j - \chi)) \\ & + e^\intercal g(s, \chi, \hat{\chi}, u)\end{aligned} \tag{21}$$

The Lipschitz continuous term $g(s, \chi, \hat{\chi}, u)$ can be upper bounded by $||g(s, \chi, \hat{\chi}, u)|| < L_g||e||$, where L_g is the Lipschitz constant. Using the Cauchy-Schwarz inequality and Lipschitz continuity assumption of $g(s, \chi, \hat{\chi}, u)$, the upper bounds on the term $e^\intercal g(s, \chi, \hat{\chi}, u)$ can be derived as follows.

$$||e^\intercal g(s, \chi, \hat{\chi}, u)|| \leq L_g||e||^2 \tag{22}$$

Since the history stack is complete, $\sum_{j=1}^{M-1} \Omega(s_j, v_j)\Omega^\intercal(s_j, v_j) > 0$, the summation term in (21) containing $(\chi_j - \chi)$ can be upper bounded using the the Cauchy-Schwarz inequality as follows

$$\sigma_1^2(||\sum_{j=1}^{M}(\chi_j - \chi)||) \tag{23}$$

where σ_1^2 is the smallest singular value of $\sum_{j=1}^{M}\Omega\Omega^T$.

Using (22) and (23), $\dot{V}$ in (21) can be modified to

$$\begin{aligned}\dot{V} \leq & -\bar{K}\sigma_1^2||e||^2 + \bar{K}\sigma_1^2 M\bar{\chi}||e|| \\ & + L_g||e||^2 \qquad (24) \\ \leq & -(\bar{K}\sigma_1^2 - L_g)||e||^2 \qquad (25) \\ & + \bar{K}\sigma_1^2 M\bar{\chi}||e||\end{aligned}$$

The following gain condition needs to be satisfied

$$\bar{K} > \frac{L_g}{\sigma_1^2} \tag{26}$$

then (26) can be written as

$$\dot{V} \leq -k_2||e||^2 + k_3||e|| \tag{27}$$

where $k_2 = \bar{K}\sigma_1^2 - L_g$. Adding and subtracting $\theta||e||^2$ in (27), yields

$$\begin{aligned}\dot{V} \leq & -\bar{k}_2||e||^2 - \theta||e||^2 + k_3||e|| \\ \leq & -\bar{k}_2||e||^2 \qquad \forall||e|| \geq \frac{k_3}{\theta}\end{aligned} \tag{28}$$

where $\bar{k}_2 = k_2 - \theta$ and $0 < \theta < 1$. Now, using the upper and lower bounds on $V(e)$, (28), and invoking Theorem 4.18 in [29], the error $\|e(t)\|$ is uniformly ultimately bounded with an ultimate bound according to Theorem 4.18. ■

Remark 3. The gain $\bar{K}$ can be chosen to minimize the disturbance caused due to $e^\intercal g(s, \chi, \hat{\chi}, u)$. Although the presented analysis contains only two cases, i.e., before and after the history stack is full, new data can be continuously added to the stack after the history stack is full. Using the Algorithm I, data is continuously added after the history stack is full, hence, the upper bound on the derivative of the Lyapunov function holds for all time after the history stack is full. Thus, (18) is a common Lyapunov function (cf. [30]).

Algorithm 1: Depth Estimation using Concurrent Learning

Data: State vector s and velocity vector $u = [v, \omega]^\intercal$
Result: Estimates $\hat{\chi}$
Initialize $\hat{\chi}, M$;
Define the observer gain $\bar{K}$;
Initialize the History Stack and the Auxiliary Stack $\mathcal{H}, \mathcal{G}$ with zeros of size $M-1$ and N respectively;
while *data for the current time step is present* **do**
  Measure the linear and angular velocity of the camera v, ω;
  Compute feature points and create state vector s;
  Compute $\dot{\kappa}, \beta$ using equations (15)-(16);
  Integrate $\dot{\kappa}$ and calculate $\hat{\chi}$ using equation (14);
  if *Number of iterations* < M **then**
    Add data point to History Stack $\mathcal{H}$;
  end
  Add data point to G in a cyclic way;
  Search for $M-1$ data points with maximum σ_1^2 in the G stack;
  Replace data in $\mathcal{H}$ with the selected $M-1$ points from $\mathcal{G}$;
end

VI. Simulation Results

A simulation was performed using a single feature point to verify the performance of the observer designed in Section III. An initial global point is selected as $m(t_0) = [1, 1, 1]^\intercal$

where $m = [X, Y, Z]^\intercal$. An auxiliary state vector $y(t) = [y_1(t), y_2(t), y_3(t)]^\intercal = [\frac{X}{Z}, \frac{Y}{Z}, \frac{1}{Z}]^\intercal$ is constructed for the measurement of the inverse depth $\chi = \frac{1}{Z}$. The trajectories are simulated by integrating the equation given in (5) and (6), where $v = [v_X, v_Y, v_Z]^\intercal$ are the linear velocities and $\omega = [\omega_X, \omega_Y, \omega_Z]^\intercal$ are the angular velocities. From the mathematics presented in Section II, state vector is defined as $s = [y_1(t), y_2(t)]^\intercal$ and $\chi = y_3$. The state s, in this case, is completely measurable in terms of pixel co-ordinates and can be converted into normalized image plane co-ordinates.

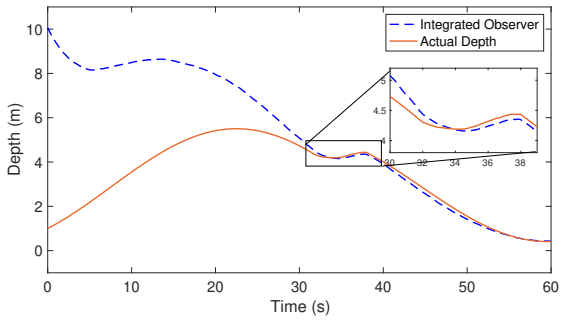

Figure 1. Comparison between the actual depth and estimated depth over a period of 60 seconds

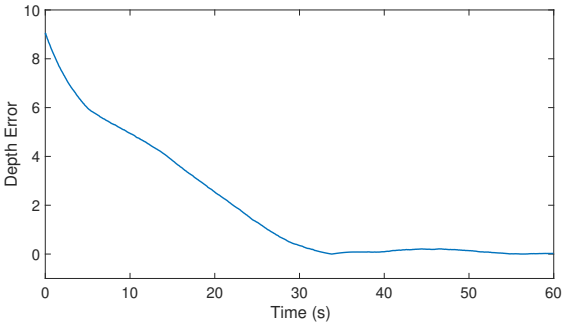

Figure 2. Error between the true and the estimated depth over time

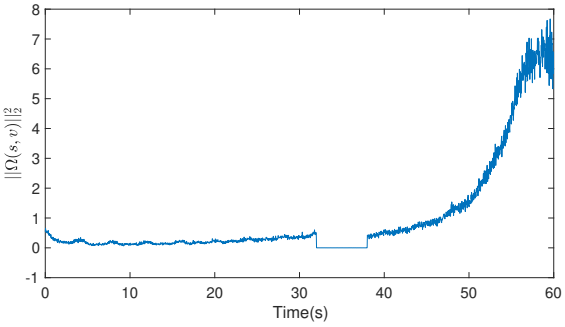

Figure 3. Evolution of $||\Omega(s, v)||^2$ over time with loss of excitation from 31 to 36s

A fourth order Runge-Kutta integrator with a fixed time-step of 0.03s is used to integrate the equations and generate trajectories for all values of $y(t)$. The time-step is so chosen that is matches the real camera frequency of 30Hz. The velocities used for simulating the feature trajectories are

Table I
CONVERGENCE AND ERROR STATISTICS OF THE DESIGNED OBSERVER.

Convergence Time(s)	MAPE	RMSE
33.45	79.46	2.45

$$v = [0.3, 0.2cos(\frac{\pi t}{4}), -0.3]^\intercal \tag{29}$$

$$\omega = [0, -\frac{\pi}{30}, 0]^\intercal \tag{30}$$

The integration is carried out from 0 to 31s. A special case of velocities is used later to make $h_1^2 + h_2^2 = ||\Omega(s, v)||^2 = 0$ over a period of 5s. The end state of the first integration is the initial state for these velocities. Velocities are chosen such that $(h_1^2 + h_2^2) = 0$ which implies $h_1 = 0$ and $h_2 = 0$. Simplifying (7) we have, $v_X = y_1 \times v_Z$ and $v_Y = y_2 \times v_Z$. The linear velocity in the Z direction is chosen to be $v_Z = 0.1\cos(\frac{\pi t}{4})$. As a result, the whole velocity vector is

$$v = [0.1\cos(\frac{\pi t}{4}) \times y_1(t), 0.1\cos(\frac{\pi t}{4}) \times y_2(t), 0.1\cos(\frac{\pi t}{4})]^\intercal$$
$$\omega = [0, 0, 0]^\intercal$$

The integration is carried out after 31s over a period of 5s such that $||\Omega(s, v)||^2 = 0$. After 36s the same velocities are used as in (29) and (30) to simulate the trajectories until 60s. Additive white Gaussian noise with a signal to noise ratio (SNR) of 20 dB is added to the state during integration, and noise with a variance of .01 and zero mean is added to the velocity signal. The observer gain $\bar{K}$ is set to 0.0009. The initial value for the inverse depth estimate is set to $\hat{\chi}(t_0) = 0.1$ which corresponds to a depth of 10m. The history stack and the auxiliary stack are initialized with 120 points and 150 points respectively for the purpose of simulation. The results of the simulation are summarized by the plots shown in Figs. 1-3.

Fig. 1 shows the value of the actual depth compared with the estimated depth. The estimated depth converges to the true depth even when the signal is not exciting between 31 to 36s. This can be attributed to the use of a history stack which makes updates to the estimate based on previous data when the trajectories are not informative. Fig 2. shows the depth error which keeps reducing even when the value of $||\Omega(s, v)||^2$ is low (<1) and the depth error goes to zero even when the excitation is not present (as $||\Omega(s, v)||^2$ is 0 over a period of 5s). Fig 3. shows the evolution of the $||\Omega(s, v)||^2$ over time with the peak value at $\sim$ 58s.

Table I. explains the error statistics in terms of root mean square error (RMSE), mean absolute percent error (MAPE) and convergence time. The higher MAPE and RMSE are due to the initial conditions which are far from the true value. The observer estimate converges at 33.45s when excitation is not present between 31s to 36s.

VII. Conclusion

A concurrent learning based reduced order observer is presented for estimating the depth of a stationary feature point in an image using a moving camera. The estimation error is shown to be UUB. The simulation result shows the performance of the designed observer in the presence of noise and when the PE condition is violated. The convergence of the observer when excitation is not present is demonstrated and the RMSE, MAPE metrics provided show the efficiency of the observer.

References

[1] C. Godard, O. Mac Aodha, and G. J. Brostow, "Unsupervised monocular depth estimation with left-right consistency," in *CVPR*, vol. 2, no. 6, 2017, p. 7.

[2] R. Spica and P. R. Giordano, "A framework for active estimation: Application to structure from motion," in *IEEE Conference on Decision and Control, CDC'13*, 2013.

[3] R. Spica, P. R. Giordano, and F. Chaumette, "Active structure from motion: Application to point, sphere, and cylinder," *IEEE Transactions on Robotics*, vol. 30, no. 6, pp. 1499–1513, 2014.

[4] ——, "Coupling visual servoing with active structure from motion," in *IEEE Int. Conf. on Robotics and Automation, ICRA'14*, 2014.

[5] R. Spica, P. Robuffo Giordano, and F. Chaumette, "Coupling active depth estimation and visual servoing via a large projection operator," *The International Journal of Robotics Research*, vol. 36, no. 11, pp. 1177–1194, 2017.

[6] S. Soatto and P. Perona, "Reducing Structure from Motion": a general framework for dynamic vision. 1. modeling," *IEEE Transactions on Pattern Analysis and Machine Intelligence*, vol. 20, no. 9, pp. 933–942, 1998.

[7] L. Matthies, T. Kanade, and R. Szeliski, "Kalman filter-based algorithms for estimating depth from image sequences," *International Journal of Computer Vision*, vol. 3, no. 3, pp. 209–238, 1989.

[8] H. Kano, B. Ghosh, and H. Kanai, "Single camera based motion and shape estimation using extended kalman filtering," *Mathematical and Computer Modelling*, vol. 34, no. 5-6, pp. 511–525, 2001.

[9] A. Chiuso, P. Favaro, H. Jin, and S. Soatto, "Structure from motion causally integrated over time," *IEEE transactions on pattern analysis and machine intelligence*, vol. 24, no. 4, pp. 523–535, 2002.

[10] M. Jankovic and B. K. Ghosh, "Visually guided ranging from observations of points, lines and curves via an identifier based nonlinear observer," *Systems & Control Letters*, vol. 25, no. 1, pp. 63–73, 1995.

[11] D. Karagiannis and A. Astolfi, "A new solution to the problem of range identification in perspective vision systems," *IEEE Transactions on Automatic Control*, vol. 50, no. 12, pp. 2074–2077, 2005.

[12] W. E. Dixon, Y. Fang, D. M. Dawson, and T. J. Flynn, "Range identification for perspective vision systems," in *Proc. Am. Control Conf.*, Denver, Colorado, June 2003, pp. 3448–3453.

[13] O. Dahl, F. Nyberg, and A. Heyden, "Nonlinear and adaptive observers for perspective dynamic systems," in *American Control Conference, 2007. ACC'07.* IEEE, 2007, pp. 966–971.

[14] X. Chen and H. Kano, "State observer for a class of nonlinear systems and its application to machine vision," *IEEE Transactions on Automatic Control*, vol. 49, no. 11, pp. 2085–2091, 2004.

[15] A. De Luca, G. Oriolo, and P. B. Giordano, "Feature depth observation for image-based visual servoing: Theory and experiments," *Int J Robot Res*, vol. 27, no. 10, pp. 1093–1116, 2008.

[16] F. Morbidi and D. Prattichizzo, "Range estimation from a moving camera: an immersion and invariance approach," in *Robotics and Automation, 2009. ICRA'09. IEEE International Conference on*. IEEE, 2009, pp. 2810–2815.

[17] A. Dani, N. Fisher, and W. E. Dixon, "Single camera structure and motion," *IEEE Transactions on Automatic Control*, vol. 57, no. 1, pp. 241–246, 2012.

[18] A. Dani, N. Fischer, Z. Kan, and W. Dixon, "Globally exponentially stable observer for vision-based range estimation," *Mechatronics*, vol. 22, no. 4, pp. 381–389, 2012.

[19] A. P. Dani, S.-J. Chung, and S. Hutchinson, "Observer design for stochastic nonlinear systems via contraction-based incremental stability," *IEEE Transactions on Automatic Control*, vol. 60, no. 3, pp. 700–714, 2015.

[20] G. Chowdhary, T. Yucelen, M. Muhlegg, and E. N. Johnson, "Concurrent learning adaptive control of linear systems with exponentially convergent bounds," *International Journal of Adaptive Control and Signal Processing*, vol. 27, no. 4, pp. 280–301, 2013.

[21] R. Kamalapurkar, B. Reish, G. Chowdhary, and W. E. Dixon, "Concurrent learning for parameter estimation using dynamic state-derivative estimators," *IEEE Transactions on Automatic Control*, vol. 62, no. 7, pp. 3594–3601, 2017.

[22] M. Muhlegg, G. Chowdhary, and E. Johnson, "Concurrent learning adaptive control of linear systems with noisy measurements," in *AIAA Guidance, Navigation, and Control Conference*, 2012, p. 4669.

[23] G. Chowdhary and E. Johnson, "Concurrent learning for convergence in adaptive control without persistency of excitation," in *Decision and Control (CDC), 2010 49th IEEE Conference on*. IEEE, 2010, pp. 3674–3679.

[24] A. Parikh, R. Kamalapurkar, H.-Y. Chen, and W. E. Dixon, "Homography based visual servo control with scene reconstruction," in *Decision and Control (CDC), 2015 IEEE 54th Annual Conference on*. IEEE, 2015, pp. 6972–6977.

[25] Z. Bell, A. Parikh, J. Nezvadovitz, and W. E. Dixon, "Adaptive control of a surface marine craft with parameter identification using integral concurrent learning," in *Decision and Control (CDC), 2016 IEEE 55th Conference on*. IEEE, 2016, pp. 389–394.

[26] G. Chowdhary and E. Johnson, "Theory and flight test validation of long term learning adaptive flight controller," in *AIAA Guidance, Navigation and Control Conference and Exhibit*, 2008, p. 6781.

[27] R. Kamalapurkar, "Simultaneous state and parameter estimation for second-order nonlinear systems," in *Decision and Control (CDC), 2017 IEEE 56th Annual Conference on*. IEEE, 2017, pp. 2164–2169.

[28] F. Chaumette and S. Hutchinson, "Visual servo control. I. basic approaches," *IEEE Robotics & Automation Magazine*, vol. 13, no. 4, pp. 82–90, 2006.

[29] H. K. Khalil, *Nonlinear Systems*, 3rd ed. Prentice Hall, 2002.

[30] D. Liberzon, *Switching in systems and control*. Springer Science & Business Media, 2003.